

Dynamic load frequency control for high-penetration wind power considering wind turbine fatigue load

Xiaodong Wang, Yingwei Wang*, Yingming Liu

Institute of Electrical Engineering, Shenyang University of Technology, Shenyang 110870, China

ARTICLE INFO

Keywords:

Load frequency control
Power system
Wind turbine
Fatigue load

ABSTRACT

The frequency stability of power systems can be improved by the participation of high-penetration wind power in grid frequency regulation. However, the wind turbine (WT) fatigue load will be increased after the wind power participates in the load frequency control (LFC). This paper proposes a control method that takes into account the WT fatigue load and the frequency response of the power system. First, wind turbines are added to the two-areas LFC model including thermal power and hydropower models to participate in frequency regulation. And considering the fatigue load experienced by the tower bending moment and the low-speed shaft torque of the WT, a WT model capable of reflecting the main dynamics is established. Then, the model identification adaptive Proportional-Integral-Differential (PID) controller is designed to be applied to LFC of wind power participating in the grid considering both frequency response and fatigue load. In order to achieve better control effects, the differential evolution (DE) algorithm is used to optimize the PID parameters based on multi-cost functions. The controller parameters are optimized by considering both the fatigue load and frequency deviation. To verify the effectiveness of the proposed method, the controller is applied to the established model and the simulation results are compared.

1. Introduction

In recent years, wind power has developed rapidly and wind power installed capacity has continued to rise [1,2]. However, they are connected to the grid by power electronic converters, which isolate the generators from the grid [3–5]. Due to the unique structure and operation of the WT, it does not have the same frequency response capability as a synchronous generator [6,7]. The grid connection of a large number of WTs is not conducive to the frequency stability of the power system, and to some extent, it has caused the wind to abandon. With the increase of wind power penetration rate, the influence of wind power on the system frequency is increasing [8,9]. In this case, the WT needs to provide frequency regulation capability through derating power generation and participate in grid frequency regulation when it has frequency regulation capability. However, when WTs participate in grid frequency regulation, their output power needs to frequently be changed to cope with the frequency variation of the grid, which makes WT frequently pitched to increase the fatigue loads [10,11]. In the method of wind power participation in frequency regulation, the fatigue load of the WT is less considered [12–14]. Therefore, it is necessary to study a control method that takes into consideration both the load frequency control performance and the WT fatigue load.

Some methods have been proposed for wind power to participate in frequency regulation. The concept of virtual inertia was first proposed in the literature [15]. The virtual control link is used to support the frequency regulation, so that the rotor kinetic energy can be released to support the frequency regulation. In [16], a variable coefficient combined virtual inertia control strategy for doubly fed induction generators (DFIG) to participate in frequency regulation is proposed. Virtual inertial control is used to suppress rapid frequency changes caused by load disturbances in the system. After the rotor speed changes, the rotor kinetic energy control loses its adjustment capability, and its adjustment time generally does not exceed 6 s [17]. In order to simulate the power-frequency static characteristics of the primary frequency regulation of the synchronous generator, the droop control method is proposed. The WT output power is adjusted according to frequency deviation. A droop control method based on the de-loading level setting control coefficient is proposed in [18]. The frequency performance of WTs under different wind conditions can be at a superior level. A method of introducing a damping control link into the conventional droop control loop to improve the system frequency stability is proposed in [19], which the problem of interference stability is reduced. Compared with the virtual inertia control, the frequency deviation is introduced by the droop control, which near the lowest frequency can

* Corresponding author.

E-mail address: 13322482011@163.com (Y. Wang).

be supported stronger, but the response speed is slower than the virtual inertia control.

In the recent research on LFC models, different wind farm droop control methods were introduced to overcome the above problems. A coordinated distributed model predictive control (DMPC) for the LFC of a power system is proposed in [20]. The proportional–integral–derivative (PID) droop control method of interconnected multi-area power systems is proposed in [21]. The frequency control performance can be achieved better by these two methods. The self-tuning fuzzy-based PID droop is proposed for instead of the fixed PID droop in de-loaded area to improve the frequency excursions in [22,23]. Besides, the intelligent algorithms like particle swarm optimization (PSO), artificial bee colony (ABC) and symbiotic organisms search (SOS) are used to optimize the fuzzy membership functions and PID parameters based on multi-cost functions. However, these researches only consider the frequency response performance, and the WT fatigue loads are ignored.

Frequency regulation performance and WT fatigue load are considered simultaneously. This paper proposes a model identification adaptive PID droop control method to replace the constant droop in the traditional LFC to participate in the frequency regulation of the grid. Since the performance of the controller depends largely on the parameters of the PID, the parameters are optimized using the DE algorithm. To test controller performance, various simulations were performed on the MATLAB/Simulink platform, including load changes, system parameter changes, different wind conditions. The simulation results show that the frequency regulation performance and the WT fatigue load can be both taken into consideration by the proposed control method. And the frequency regulation capability of wind power in different wind speed sections is analyzed.

The main contributions of this paper are as follow:

- 1) A novel WT model for LFC considering fatigue load is established.
- 2) A novel LFC method based on model identification adaptive PID is proposed for frequency regulation of wind power participation in the power grid.
- 3) Fatigue load and frequency response are considered simultaneously, PID parameters are optimized based on DE algorithm.
- 4) The wind conditions with different turbulence and average speed are used to analyze the performance of the controller and the ability of wind power to participate in frequency regulation.

2. Power system model for conventional LFC

The dynamic models of multi-area interconnected power system are established to design and optimize the appropriate controllers under MATLAB/SIMULINK environment. To study the frequency regulation performance of WTs, it is necessary to add reheat thermal power and hydropower to the model.

2.1. Conventional generator model

The conventional genset models for simulation can be seen in Fig. 1. Considering the specific literature, they are modeled according to the simplified governor-based models widely used and proposed in [24].

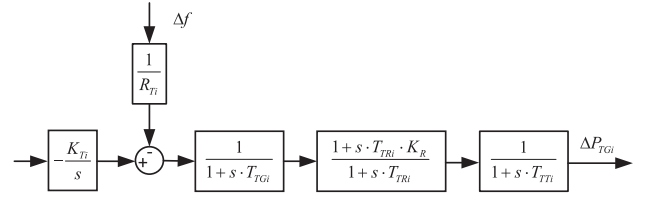
Parameters for conventional power plant are listed in Table 1, and the values are referred to literature [25].

2.2. Multi-area power system model

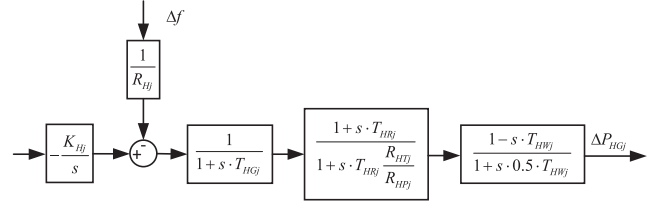
A two-area LFC model with wind power plant is shown in Fig. 2. The frequency deviation under load imbalance conditions is usually based on the following function:

$$\Delta f_i = \frac{1}{2H_i s + D_i} \sum (\Delta P_i) \quad (1)$$

where, H_i is the equivalent inertia constant of the area i power system,



a. Block diagram of thermal power plant model.



b. Block diagram of hydro power plant model.

Fig. 1. Conventional genset models for simulation.

Table 1
Parameters for conventional power plant.

Parameter	Name	Value(pu)
K_{Ti}	Integral controller for thermal plant model	2.00
R_{Ti}	Speed droop for thermal plant model	0.05
T_{TGi}	Speed governor for thermal plant model	0.20
T_{TRe}	Time constant of reheater	7.00
K_{Re}	Fraction of power generated by high pressure section	0.30
T_{TTi}	Time constant of main inlet volumes and steam chest	0.30
K_{Hj}	Integral controller for hydro-power plant model	2.00
R_{Hj}	Speed droop for hydro-power plant model	0.05
T_{HGj}	Speed governor for hydro-power plant model	0.20
T_{HRj}	Reset time	5.00
R_{HTj}	Temporary droop	0.38
R_{HPj}	Permanent droop	0.05
T_{HWj}	Water starting time	1.00

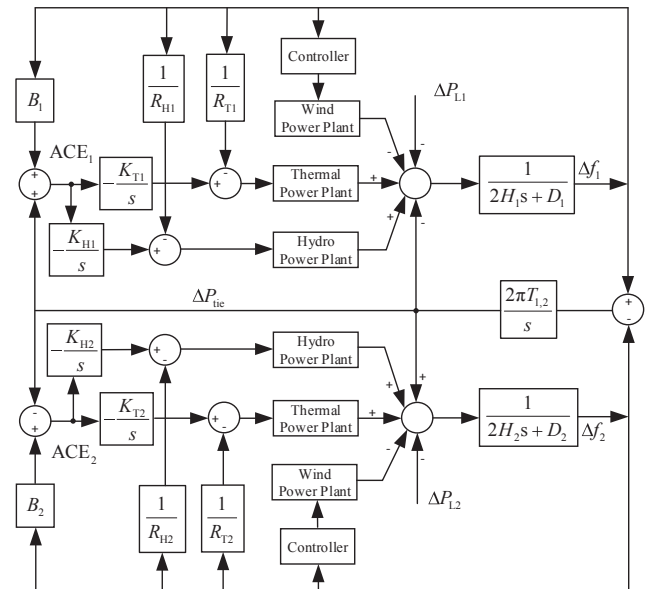


Fig. 2. Two-area LFC model with wind power plant.

D_i is the equivalent damping factor of the loads, ΔP_i is the power deviation

The transmission level voltage is usually considered by the

connection line for multi-area interconnection purposes. The power exchange and frequency of the tie line can vary depending on the load demand. The tie line power exchange ΔP_{tie} between the two areas is determined by the following equation:

$$\Delta P_{tie} = \frac{2\pi T_{1,2}}{s} (\Delta f_1 - \Delta f_2) \quad (2)$$

where, $T_{1,2}$ is the synchronizing moment coefficient of the tie-line between 1 and 2 areas.

In the process of conventional power grid frequency regulation, the balance between the interconnected power systems is determined by generating an area control error signal (ACE) when a frequency deviation exists. ACE can be calculated by the following equation:

$$ACE_i = B_i \Delta f_i + \sum \Delta P_{tie} \quad (3)$$

where, B_i is the bias-factor.

3. Wind turbine model for load frequency control considering fatigue load

In this study, the fatigue load of WT is considered, so the WT model used for LFC should not only reflect the output characteristics of wind farms in power systems but also reflect the main dynamics of the WT. The WT model is established referring to the NREL5MW model [26], and the WT block diagram can be seen from Fig. 3. It consists mainly of eight parts.

Torque control and pitch control are included in the WT controller. Its main task is to make the WT's output power tracking power input command. Torque control block diagram can be seen from Fig. 4.

Generator torque reference T_{dem1} can be obtained by lookup table related to measured generator speed ω_{g_meas} . T_{dem2} can be obtained by the equation $T_{dem2} = P_{dem}/\omega_{g_meas}$. Generator torque reference T_{g_ref} can be obtained by T_{dem1} and T_{dem2} by torque selector. When the WT is not pitch, the torque T_{ref} is T_{dem1} . When the WT is pitched, the torque T_{ref} is T_{dem2} . There are three main types of WT pitching situation: Captured wind energy exceeds demand power; The generator speed exceeds the set speed; To prevent integral saturation.

Pitch control block diagram can be seen from Fig. 5. Where, ω_{g_rated} is the rated generator speed. ω_{g_error} is the deviation of generator speed. The PI control method as shown in Fig. 5 is the simple pitch control method. β_{ref} is the pitch angle reference, it will change as ω_{g_error} changes because of PI controller.

Where, $K_{p\theta}$ and $K_{i\theta}$ are the coefficients of the PI controller.

The pitch actuator is a simulation of the actual pitch action. Its block diagram can be seen from Fig. 6.

Where, $K_{p\theta}$ and $K_{i\theta}$ are parameters of PI pitch control respectively. K_{pa} is the gain factor for Pitch actuator, T_{pa} is the hydraulic time constant.

The aerodynamic torque T_r is expressed by:

$$T_r = \frac{0.5\pi R_b^2 \rho v^3 C_p}{\omega_r} \quad (4)$$

where, ρ is the air density; v is the wind speed; R_b is the length of the

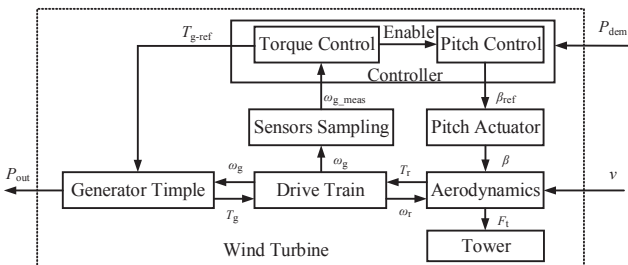


Fig. 3. Wind turbine block diagram.

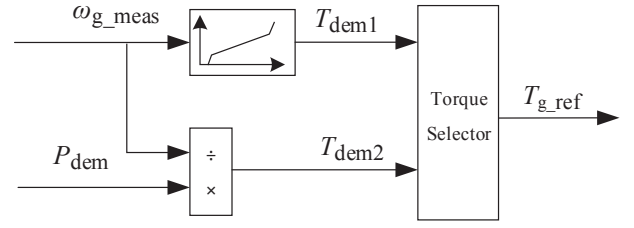


Fig. 4. Torque control block diagram.

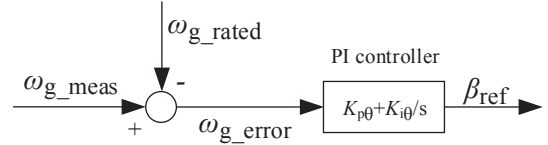


Fig. 5. Pitch control block diagram.

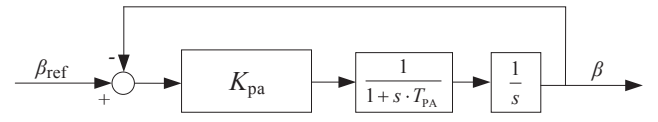


Fig. 6. Pitch actuator block diagram.

blade; C_p is the power coefficient; ω_r is rotor speed.

Basically, non-dimensional curves of power coefficient C_p can be expressed by a function of tip speed ratio λ and the blade angle β like Eq. (5).

$$C_p = (0.44 - 0.0167\beta) \sin \frac{\pi(\lambda-3)}{15 - 0.3\beta} - 0.00184(\lambda - 3)\beta \quad (5)$$

C_p can be obtained by lookup table too, like Fig. 7. C_p are obtained by lookup table method in this research.

The generator speed ω_g is generated by drive train of wind turbine rotor, it can be calculated by:

$$\omega_g = \eta_g (T_r - \eta_g T_g) \frac{1}{J_t \cdot s} \quad (6)$$

where, η_g is the gear box ratio, J_t is equivalent mass.

Since the dynamics of the generator are neglected, the generator torque T_g is approximately equal to its reference value.

$$T_g \approx T_{g_ref} \quad (7)$$

The drive train can be considered to be rigidly coupled and the single-mass model is used in this study, J_t is equivalent mass and it can be calculated by:

$$J_t = J_r + \eta_g^2 J_g \quad (8)$$

where, J_r is the rotor mass, J_g is the generator mass.

The fatigue loads of WT can be divided into two parts: one is external loads, and the other is internal loads. In this paper, the fatigue

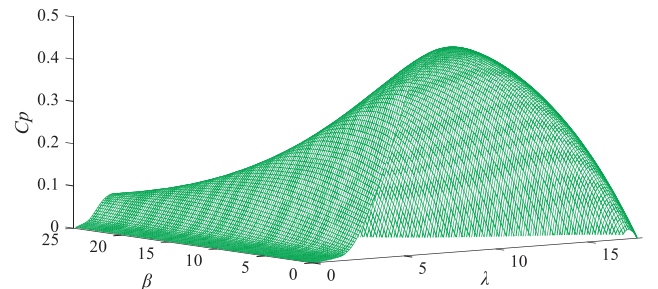


Fig. 7. C_p based on lookup table.

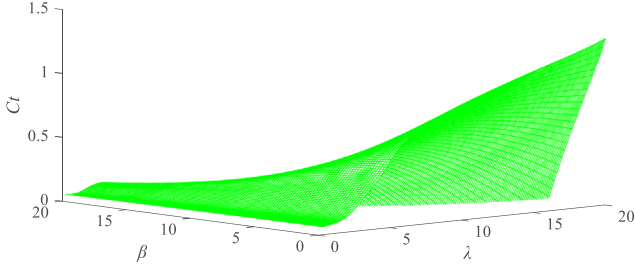


Fig. 8. C_t based on lookup table.

loads mainly focus on the torsion of the shaft and the tower deflection. Compared with static loads, the dynamic stress causing structural damage of WTs is a much bigger issue [27]. They can be expressed by shaft torque T_s and tower bending moment M_t . The shaft torque T_s twists the low-speed shaft. According to the motion equation, T_s can be expressed as:

$$T_s = T_r - J_r \dot{\omega}_r \quad (9)$$

The bending moment M_t can be evaluated by:

$$M_t = H_{tower} \cdot F_t \quad (10)$$

where, H_{tower} is the tower height.

The tower thrust force F_t can be calculated by:

$$F_t = 0.5\pi R^2 \rho v^2 C_t \quad (11)$$

where, C_t is the thrust coefficient and can be obtained by lookup table like Fig. 8.

According to reference [27], the fatigue loads experienced by shaft torque and tower bending moment are related to their fluctuation. The fatigue load can be reduced by reducing the fluctuations of T_s and M_t . Therefore, Eqs. (12) and (13) can be used to estimate the fatigue loads experienced by T_s and M_t during the time.

$$Fatigue_{T_s} = \int_{t=0}^{\infty} \Delta T_s^2(t) dt \quad (12)$$

$$Fatigue_{M_t} = \int_{t=0}^{\infty} \Delta M_t(t) dt \quad (13)$$

The output power can be expressed by:

$$P_{out} = \frac{1}{1 + s \cdot T_W} T_{g_ref} \cdot \omega_{g_meas} \quad (14)$$

where, T_W is the time constant for generator filter.

In general, incremental control methods are used for LFC model. To make it more clearly, the frequency is changed according to the change of the grid load, and then the power variation of the generator is controlled according to the change of the frequency to stabilize the frequency.

The WT has its frequency regulation capability through derating control. The output power can be altered between maximum power point tracking power P_{mpppt} and de-rated power P_{der} by changing rotor speed and generator torque. The derating factor is assumed to be γ . Therefore, the positive reserve power P_{pr+} of the wind farm can be determined by γ for frequency regulation according to the following equation.

$$P_{pr+} = P_{mpppt}(1 - \gamma) \quad (15)$$

Therefore, a block diagram of a wind farm model for LFC can be represented by Fig. 9.

As shown in Fig. 9, the use of these three WTs is to represent and calculate the incremental output form of wind power. WT1 and WT2 are used for auxiliary calculations. P_{mpppt} is generated from WT model 1. The input of WT model 1 is the maximum power generation capacity P_{max} . The positive reserve power P_{pr+} of the wind farm is generated

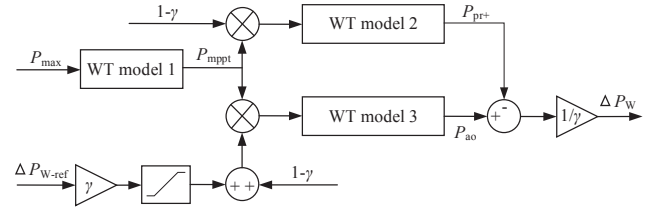


Fig. 9. Block diagram of a wind farm model for LFC.

from WT model 2. The actual output power P_{ao} generated by the wind farm is generated by WT model 3. Therefore, the power deviation generated by the wind farm can be calculated by P_{pr+} and P_{ao} .

4. Model identification adaptive PID control using DE algorithm to optimize parameters

In order to adapt to the uncertainty and nonlinearity between wind power and power grid, a model identification adaptive PID control method is proposed, and DE algorithm is used to optimize PID parameters. An online model identification method to obtain time-varying system parameters of the controlled plant is used to the adaptive model identification PID control. The range of PID parameters can be changed by the identified system parameters. In order to make the control effect better, the PID initial parameters should be ascertained by a well-mechanism. In this case, DE algorithm is used to perform the above determination mechanism. The control method is shown in Fig. 10.

As shown in Fig. 10, two different loops are included. The control loop is used to control the system frequency deviation, and the parameter optimization loop is used to adjusted the parameters of the PID based on the cost function.

4.1. Model identification adaptive PID control method

Method of model identification is incorporated with control strategy. Forgetting factor recursive least squares (FFRLS) method can be applied to constant uncertain systems [28]. In general, the FFRLS method is used to identify the parameters of the transfer function below:

$$\begin{aligned} \mathbf{A}(z^{-1})\mathbf{y}(k) &= \mathbf{B}(z^{-1})\mathbf{u}(k - d) \\ \mathbf{A}(z^{-1}) &= 1 + a_1z^{-1} + \dots + a_{n_a}z^{-n_a} \\ \mathbf{B}(z^{-1}) &= b_0 + b_1z^{-1} + \dots + b_{n_b}z^{-n_b} \end{aligned} \quad (16)$$

where, \mathbf{y} is the output value, \mathbf{u} is the control value; n_a , n_b and d are integers related to the structure of the model. Eq. (16) can be rewritten as:

$$\begin{aligned} \mathbf{y}(k) &= -a_1\mathbf{y}(k - 1) - \dots - a_{n_a}\mathbf{y}(k - n_a) \\ &+ b_0\mathbf{u}(k - d) + \dots + b_{n_b}\mathbf{u}(k - d - n_b) \\ &= \boldsymbol{\varphi}^T(k)\boldsymbol{\theta} \end{aligned} \quad (17)$$

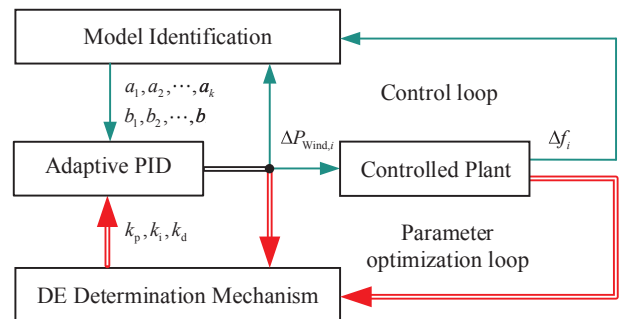


Fig. 10. Model identification adaptive PID control using differential evolution algorithm to optimize parameters.

where, φ is the data vector, θ is the parameter vector to be estimated. They can be expressed as:

$$\varphi(k) = [-\mathbf{y}(k-1), \dots, -\mathbf{y}(k-n_a), \mathbf{u}(k-d), \dots, \mathbf{u}(k-d-n_b)]^T$$

$$\theta = [a_1, \dots, a_{n_a}, b_0, \dots, b_{n_b}]$$

The formula for FFRLS parameter estimation can be expressed as:

$$\hat{\theta}(k) = \hat{\theta}(k-1) + \delta(k)[\mathbf{y}(k) - \varphi^T(k)\hat{\theta}(k-1)] \quad (18)$$

where, $\delta(k)$ can be calculated by:

$$\delta(k) = \frac{\mu(k-1)\varphi(k)}{\psi + \varphi^T(k)\mu(k-1)\varphi(k)} \quad (19)$$

where, $\mu(k)$ can be calculated by:

$$\mu(k) = \frac{1}{\psi} [E - \delta(k)\varphi^T(k)]\mu(k-1) \quad (20)$$

where, ψ is the forgetting factor.

The initial values of $\mu(0)$ and $\hat{\theta}(0)$ need to be determined before calculation. In general, their initial values can be determined by the following formula:

$$\begin{cases} \delta(0) = \zeta E \\ \hat{\theta}(0) = \varepsilon \end{cases} \quad (21)$$

where, ζ is the huge positive number; ε is the very small positive real vector.

The identified parameters are used for PID controller and the controller block diagram is shown in Fig. 11.

The adaptive PID control method is shown in Fig. 11. The identified system parameters are used to change the range of the PID after calculation. The parameters of PID are optimized by DE algorithm.

4.2. PID control parameter optimization method considering fatigue load using DE algorithm

The differential evolution algorithm was proposed in 1997 by Rainer Storn and Kenneth Price on the basis of evolutionary ideas such as genetic algorithms. Its essence is a multi-objective optimization algorithm that is used to solve the global optimal solution in multi-dimensional space [29,30]. The calculation process of the basic differential evolution algorithm can be seen in the Appendix A. The DE algorithm flow used in this study is shown in Fig. 12.

It is characterized by an approximate optimal solution without the need to accurately model the optimized object. Its main advantages compared with genetic algorithms (GA) and particle swarm optimization (PSO) are as follows:

1) Parameter setting problem

In the DE algorithm, there are mainly two parameters that need to be adjusted, and the parameter setting has little effect on the result. There are too many parameters in the GA and PSO algorithms, and different parameter settings have a greater impact on the final result. In practical applications, the parameters have to be continuously adjusted, which increases the difficulty of using the algorithm.

2) High dimensional problem

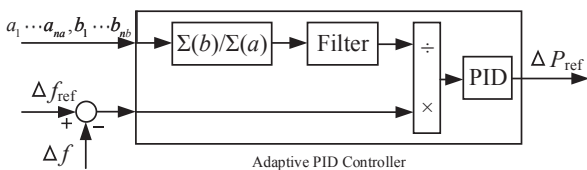


Fig. 11. Block diagram of Adaptive PID Controller.

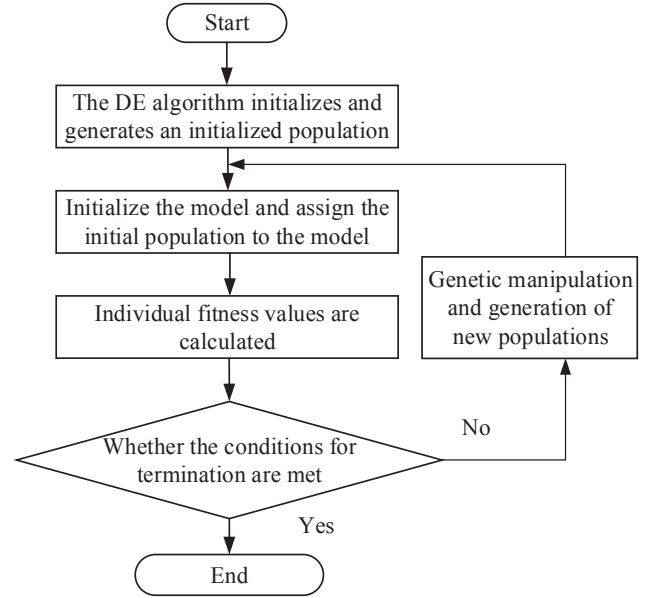


Fig. 12. The process of DE algorithm optimizing PID parameters.

GA converges slowly or even hardly on high-dimensional problems, but PSO and DE can solve it well. Especially the DE algorithm, the convergence speed is fast and the result is very accurate. In practical problems, since the vector dimension transformed into an individual is very high, the ability of the algorithm to deal with high-dimensional problems is very important. Only when the high-dimensional problem is well handled, the algorithm can be applied to practical problems. The PID parameter optimization problem of the two areas power system in this study is a 6-dimensional problem. And as the power system area increases, the dimension of the optimization problem will increase significantly, so the application of the DE algorithm is necessary.

3) Convergence performance

DE and PSO algorithms converge faster compared with GA. However, PSO is easy to fall into local optimal solution, and the algorithm is unstable.

4.3. Cost function

The reference power is frequently changed because the WT participates in frequency regulation. This will cause the pitch angle to change frequently, thereby increasing the fatigue load of the WT. In this study, the two most influential fatigue loads of the WT are considered. The background of fatigue loads has been introduced in the Chapter 3 before the article. Fatigue loads are related to fluctuations in T_s and M_t . It can be simply assumed that the smaller their fluctuation, the smaller the fatigue load. That is, the smaller the integral of ΔT_s^2 and ΔM_t^2 , the smaller the fatigue load. So, the fatigue load cost function can be simply evaluated as:

$$C_{1,i} = f_{1,i}(t) = \int_{t=0}^{\infty} (\alpha_3 \Delta T_{s,i}^2 + \Delta M_{t,i}^2) dt \quad (22)$$

where, α_3 is the weight coefficient of the two fatigue loads. In this study, $\alpha_3 = 25$. $C_{1,i}$ is the fatigue cost function for area i .

In order to balance the performance of the frequency regulation with the fatigue load of the WT, the cost function of frequency deviation can be expressed as:

$$C_2 = f_2(t) = \int_{t=0}^{\infty} (\Delta f_1^2 + \Delta f_2^2 + \alpha_4 \Delta P_{tie}^2) dt \quad (23)$$

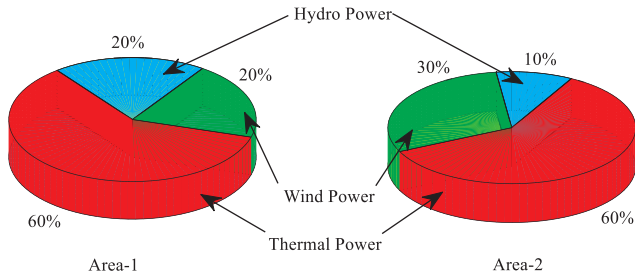


Fig. 13. The penetration for thermal power, hydro power and wind power.

where, Δf_1^2 and Δf_2^2 are the integral terms of the square of the frequency error, ΔP_{tie}^2 is the integral term of the square of the tie line power exchange. α_4 is the normalization coefficient of frequency deviation integral and tie line power deviation integral. In this study, $\alpha_4 = 1$. So, the multi-cost function is as follows:

$$\min C = \alpha_1(C_{1,1} + C_{1,2}) + (1 - \alpha_1)C_2 \quad (24)$$

where, α_1 is the weight coefficient of the cost function. The performance of fatigue load and frequency regulation is determined by α_1 .

5. Simulation results and discussions

The two-area power system model mentioned in Chapter 2 is used to evaluate power system frequency performance and WT fatigue load conditions. The penetration of thermal power, hydro power and wind power are shown in Fig. 13. Power system parameters are shown in Table 2, these parameters refer to the literature [25]. Lots of the parameters are comprehensively compared by this article, so these parameters are representative. WT parameters are shown in Table 3.

5.1. Results of controller parameters

In this study, the proposed control method is used to improve the frequency response for the power system. The parameters of FFRLS are shown in Table 4. Two step loads disturbance of 20% amplitude are applied to area-1 and area-2 at time $t = 1$ s, respectively. The average wind speed is set to 14 m/s and the turbulence intensity is set to 0.1, which the WT is allowed to generate electricity at maximum power. In order to achieve the best DE algorithm performance, different population numbers N_p and evolutionary times N_e are used for DE algorithm to optimize PID parameters. The range of N_p and N_e are 10 to 80. In this case, α_1 is considered to be 0, which is equivalent to the effect of fatigue load being ignored. Each different combination is calculated once, and the result of the cost function is shown in Fig. 14.

As shown in Fig. 14, the results of the optimization are basically same when N_p is greater than 40 and N_e is greater than 50. So, the N_p and N_e can be taken as 40 and 50 respectively considering the model simulation time and optimization performance afterwards. In order to prove that the obtained system parameters and DE algorithm parameters are optimal, the convergence curve of the DE algorithm is shown in Fig. 15. To evaluate the performance of the DE algorithm, the Particle Swarm Optimization (PSO) algorithm is used for compare in Table 5.

As shown in Table 5, it is worth noting that the optimization results

Table 2
Parameters for two-area power system.

Parameter	Name	Value(pu)
B_1, B_2	Bias factor of Area 1 and 2	0.348
D_1, D_2	The load equivalent damping factor of Area 1 and 2	1.000
H_1	Equivalent inertia constant of Area 1	2.997
H_2	Equivalent inertia constant of Area 2	3.324

Table 3
Parameters for WT.

Parameter	Name	Value
R_b	Length of blade	63 m
ρ	Air density	1.22 kg/m ³
η_g	Gear box ratio	97
J_r	Rotor mass	3.5×10^7 kg·m ²
J_g	Generator mass	5.3×10^2 kg·m ²
H_{tower}	Tower height	87.6 m
$K_{p\theta}$	PI pitch control parameters	0.2143
$K_{i\theta}$	PI pitch control parameters	0.0918
K_{pa}	the gain factor for Pitch actuator	10
T_{pa}	hydraulic time constant	0.05
T_W	Time constant for generator filter	0.2
γ	De-rated factor	0.15

Table 4
Parameters for FFRLS.

Parameter	Value
ζ	10 ⁶
ϵ	[0.1, 0.1, 0.1, 0.1, 0.1, 0.1]
ψ	0.97
n_a	3
n_b	3

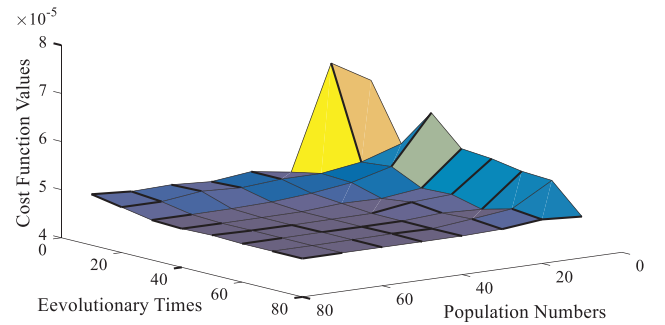


Fig. 14. DE algorithm performance under different population numbers N_p and evolutionary times N_e .

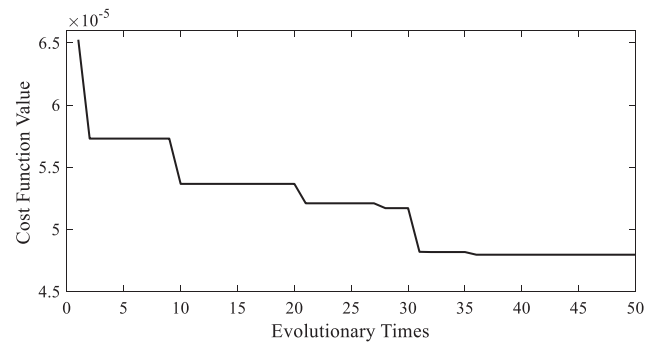


Fig. 15. Convergence curve of the DE algorithm while $N_e = 50$ and $N_p = 40$.

Table 5
Performance for the DE and PSO algorithm.

Algorithm	Cost Function Value	Percentage
DE	4.797×10^{-5}	-3.5%
PSO	4.971×10^{-5}	

Table 6
Performance for the DE and PSO algorithm.

Response		DE	PSO	Percentage
Δf_1	MPUS/Hz	5.974×10^{-3}	5.976×10^{-3}	-0.03%
	MPOS/Hz	1.086×10^{-3}	1.215×10^{-3}	-10.62%
	TS/s	5.4	7.3	-26.03%
Δf_2	MPUS/Hz	2.684×10^{-3}	2.685×10^{-3}	-0.04%
	MPOS/Hz	0	0	0
	TS/s	7.6	8.5	-10.59%
ΔP_{tie}	MPUS/Hz	1.730×10^{-3}	1.732×10^{-3}	-0.12%
	MPOS/Hz	0	0	0
	TS/s	8.9	10.8	-17.59%

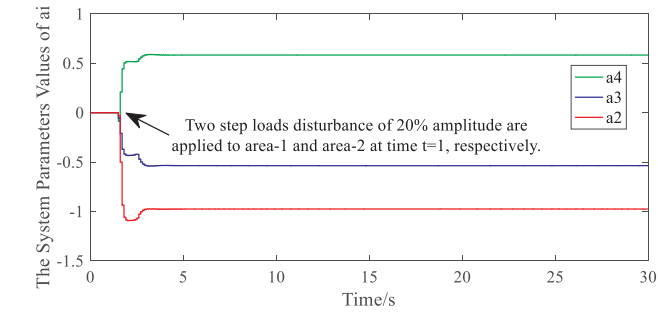
when $N_p = 40$ and $N_e = 50$ are better than those based on PSO with particle number 40 and iteration number 50.

The optimal PID parameters calculated by DE and PSO algorithms are applied to the LFC model. The transient specifications of the dynamic responses using different algorithms are indicated in Table 6. It can be seen from Table 6 that the maximum percentage undershoot (MPUS), maximum percentage overshoot (MPOS), and settling time (TS) of $\pm 0.002\%$ band have lower values using the proposed controller than that by using PSO.

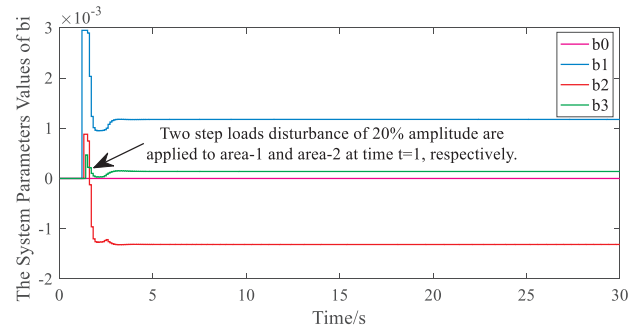
The system parameters for area 1 derived from the model identification method are shown in Fig. 16. It can be seen from Fig. 16 that the parameters of the area 1 can be well identified, which indicates that the system identification method has a good performance, so the PID control performance can be improved.

5.2. System performances under different step load fluctuations

In order to further test the performance of the controller, different step load changes are used for the model. At time $t = 1$ s, the step load fluctuations of 5%, 10%, and 15% p.u. amplitude are simultaneously applied to area 1 and 2. The frequency responses of Δf_1 and Δf_2 are shown in Fig. 17. As the load increases, transient specifications such as MPUS, MPOS, and TS will increase. These dynamic responses are within an acceptable range of frequency and power deviations.

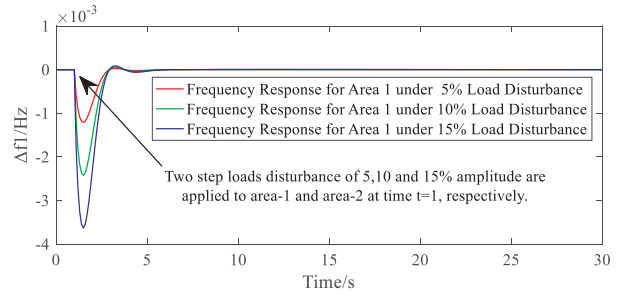


a. The system parameters of a_i for area-1

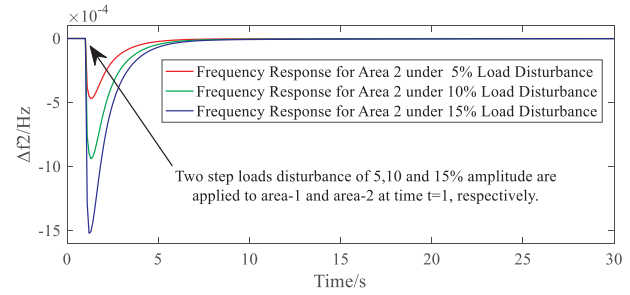


a. The system parameters of b_i for area-1

Fig. 16. The system parameters for area-1 derived from the model identification method.



a. The frequency responses for area-1 under different load disturbance.



b. The frequency responses for area-2 under different load disturbance.

Fig. 17. The frequency responses for power system under different load disturbance.

5.3. Comparison of system frequency deviation and WT fatigue load under different weight factor of cost function

Since the pitch angle is frequently changed when the WT participates in the frequency regulation, it is necessary to balance the frequency response with the fatigue load. The parameters are optimized three times after each change of α_1 considering the scattering of results of the DE algorithm, and then the optimal parameters are obtained by the smallest cost function. The Damage Equivalent Loads (DELs) of T_s and M_t when α_1 changes can be seen in Table 7. Note that the compared DELs is the accumulation of two areas DELs.

As shown in Table 7, as α_1 increases, the DELs of T_s and M_t decrease. When α_1 is 0.7, the result of the DE algorithm is that wind power does not participate in frequency regulation, and the PID parameters are all zero, and the DELs are reduced more. The DEL of T_s is reduced from 0.58% to 17.12% and the DEL of M_t is reduced from 3.54% to 36.16%. This shows that the frequency response effect and fatigue load can be changed by changing the weight factor α_1 of the cost function. The area 2 frequency response of the system when α_1 changes can be seen in Fig. 18.

As shown in Fig. 18, when the value of α_1 ranges from 0.1 to 0.5, the performance of the frequency response gradually deteriorates with the increase of α_1 , but this change is not obvious. When α_1 is 0.6, the system frequency response changes greatly. The curve with $\alpha_1 = 0.7$ is the

Table 7
The Total DELs of T_s and M_t when α_1 changes.

α_1	DEL of T_s /Nm	Percentage/%	DEL of M_t /Nm	Percentage/%
0	5,802,757		368,352,254	
0.1	5,765,796	-0.64	368,960,567	0.17
0.2	5,769,246	-0.58	355,310,501	-3.54
0.3	5,653,221	-2.58	352,452,188	-4.32
0.4	5,637,167	-2.85	344,655,785	-6.43
0.5	5,547,946	-4.39	344,308,819	-6.53
0.6	5,576,436	-3.90	344,993,804	-6.34
0.7	4,809,622	-17.12	235,156,650	-36.16

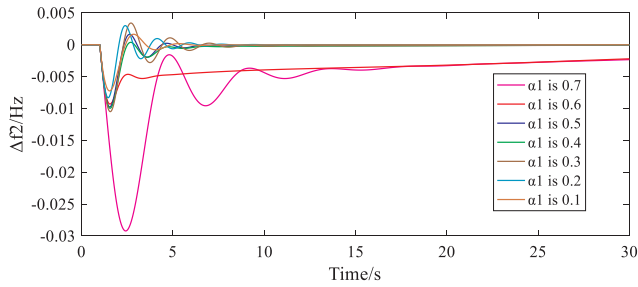


Fig. 18. Frequency regulation of area 2 under different PID parameters.

Table 8

The optimal PID parameters for $\alpha_1 = 0, 0.4, 0.7$.

α_1	K_{p1}	K_{i1}	K_{d1}	K_{p2}	K_{i2}	K_{d2}
0	392.1	258.0	117.7	398.8	198.5	27.9
0.4	42.4	45.6	1.1	62.9	53.1	0.8
0.7	0	0	0	0	0	0

system frequency response when wind power does not participate in frequency regulation. The PID parameters are selected as parameters calculated by DE algorithm when $\alpha_1 = 0.4$ considering fatigue load and frequency response comprehensively. And the PID parameters for $\alpha_1 = 0, 0.4, 0.7$ are shown in Table 8.

5.4. Comparison of wind power participation in LFC in different wind speed sections

In order to verify the effectiveness of the proposed controller in actual operation, the system is tested by using three different wind speeds. These wind speeds are characteristic wind speeds generated by SimWindFarm [31]. Their average speed (AS) and turbulence intensity (TI) are shown in Table 9. The sampling time of the wind speed is 0.1 s, and the wind speed curve of 10 min is selected as shown in Fig. 19.

Scenario 1: Performance of the system response and fatigue load under High-speed Section.

If the wind power does not participate in the system frequency regulation, then the wind power will cause interference to the system frequency like the load. Fig. 20 shows the frequency response curve of area 2 under different PID parameters shown in Table 8. When the PID parameters are all zero ($\alpha_1 = 0.7$), the wind power will be injected into the system as a grid load. Note that there is no step load disturbance in the system in this scenario.

As shown in Fig. 20, when the wind power participates in the frequency regulation process, the frequency of the system can be improved very well, and the frequency response when considering the fatigue load is within an acceptable range. In this scenario, the DELs of wind turbines under different PID parameters are shown in Table 10.

As shown in Table 10, The fatigue load experienced by T_s can be effectively reduced using the PID parameter obtained by the DE algorithm. The range of reduction is 11.62% to 32.73%. The fatigue load experienced by M_t is slightly reduced. The range of reduction is 0.55% to 0.83%. The cumulative rainflow cycles for T_s and M_t for area 1 are

Table 9

Definition of different wind speeds.

Name	AS(m/s)	TI
High-speed Section	13	0.2
Mid-speed Section	8.5	0.2
Low-speed Section	4.5	0.1

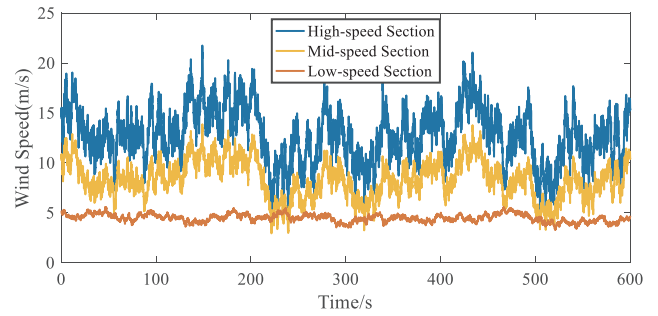


Fig. 19. Different wind speed curves.

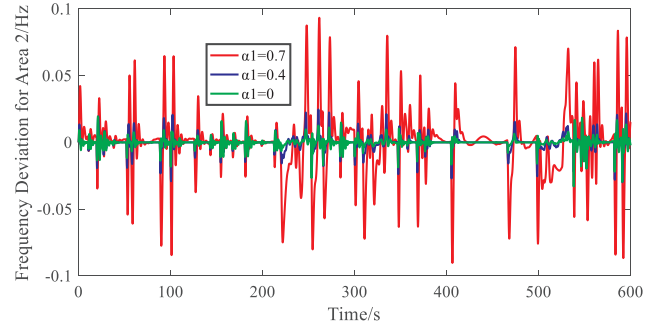


Fig. 20. Frequency performance of Area 2 with different PID parameters.

Table 10

The DELs of T_s and M_t under different PID parameters at High-speed Section.

Area	DELs for	$\alpha_1 = 0/\text{MNm}$	$\alpha_1 = 0.4/\text{MNm}$	Percentage/%
1	T_s	3.33	2.24	-32.73
	M_t	327.53	325.73	-0.55
2	T_s	2.84	2.51	-11.62
	M_t	328.33	325.59	-0.83

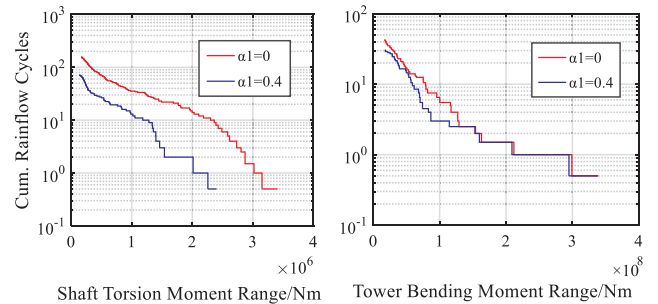


Fig. 21. The cumulative rainflow cycles for T_s and M_t for area 1 under different PID parameters.

Table 11

Average output power under different PID parameters.

Area	$\alpha_1 = 0$	$\alpha_1 = 0.4$
1	4544350 W	4550983 W
2	4515153 W	4551141 W

shown in Fig. 21, less cycles are found for the $\alpha_1 = 0.4$, which implies less fatigue loads experienced by the WT. When using different PID parameters, the average output power is as shown in Table 11, and the difference is not big. This shows that the benefit of the wind farm will not be affected.

In this scenario, the frequency regulation capability of wind power is maintained through power backup. When the de-rated factor γ is

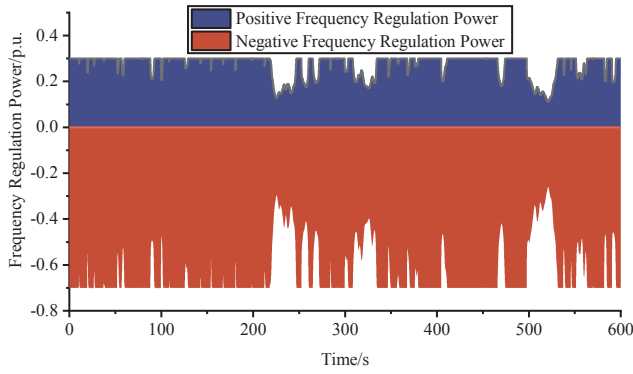


Fig. 22. The positive and negative frequency regulation power of wind power for High-speed Section.

0.15, the positive and negative frequency regulation power of wind power can be represented by Fig. 22. The curve that WT not participating in frequency regulation is shown in Fig. 20, large frequency fluctuation is caused by the high wind power penetration rate and the large enough wind speed. So, wind power should participate in LFC.

Different controller parameters are used in the model, the High-speed Section is used simultaneously by areas 1 and 2. And a random load disturbance ΔP_{L2} shown in Fig. 23 occurs in area 2. The frequency response of the area 2 is shown in Fig. 23. As shown in Fig. 23, the frequency responses are within acceptable ranges. Since the wind penetration of the area 2 is 30% and the wind speed is sufficient, it can ensure that the wind power participates in the frequency regulation with good effect. The cumulative rainflow cycles for T_s and M_t for area 2 are shown in Fig. 24, less cycles are found for the $\alpha_1 = 0.4$. The reduction of fatigue load experienced by T_s is 11.19%. The fatigue load experienced by M_t is slightly reduced. This shows that the controller has good performance for fatigue load reduction when the load fluctuates under high wind speed.

Scenario 2: Performance of the system response and fatigue load under Mid-speed Section.

The method of analysis is consistent with the method of scenario 1. The fatigue load results under different PID parameters are shown in Table 12. The result of the obtained fatigue load is similar to that of scenario 1. The fatigue load experienced by T_s can be effectively reduced and the frequency response is similar. The fatigue load experienced by M_t is reduced too.

In this scenario, when the de-rated factor γ is 0.15, the positive and negative frequency regulation power of wind power can be represented by Fig. 25. As the wind speed changes from the High-speed section to the Mid-speed Section, the frequency regulation capability of the wind power decreases. Different controller parameters are used in the model, the Mid-speed Section is used simultaneously by areas 1 and 2, and the

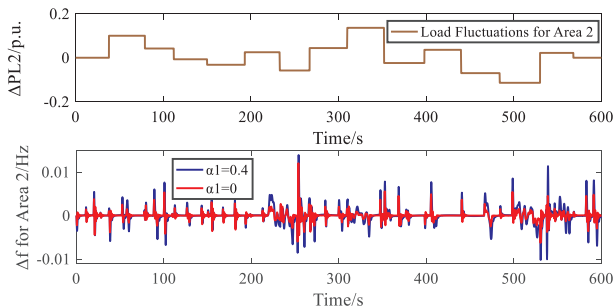


Fig. 23. Frequency performance for area 2 under load disturbances and different PID parameters under High-speed Section.

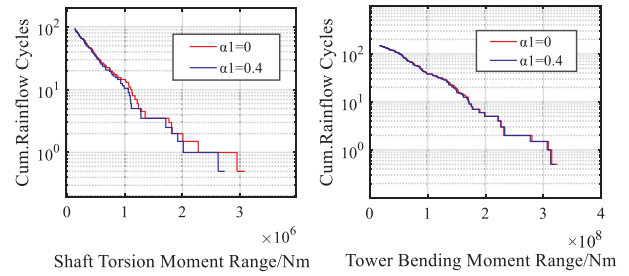


Fig. 24. The cumulative rainflow cycles for T_s and M_t for area 2 under load disturbances and different PID parameters under High-speed Section.

Table 12

The DELs of T_s and M_t under different PID parameters at Mid-speed Section.

Area	DELs for	$\alpha_1 = 0/\text{MNm}$	$\alpha_1 = 0.4/\text{MNm}$	Percentage/%
1	T_s	4.28	3.18	-25.70
	M_t	123.47	121.19	-1.85
2	T_s	3.78	3.61	-4.50
	M_t	123.48	121.48	-1.62

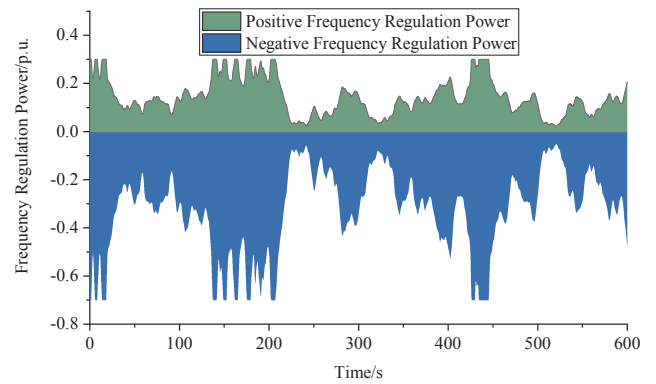


Fig. 25. The positive and negative frequency regulation power of wind power for Mid-speed Section.

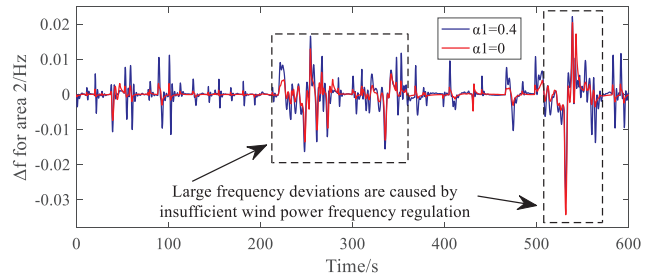


Fig. 26. Frequency performance for area 2 under load disturbances and different PID parameters under Mid-speed Section.

same random load disturbance ΔP_{L2} shown in Fig. 23 occurs in area 2. The frequency response of the area 2 is shown in Fig. 26.

As shown in Fig. 26, the frequency responses are within acceptable ranges. However, large frequency fluctuations are caused by the insufficient wind power regulation capability during $t = 220 \text{ s}$ to 360 s and $t = 500 \text{ s}$ to 570 s . When the wind power is sufficient, the frequency fluctuation can be well suppressed. The cumulative rainflow cycles for T_s and M_t for area 2 are shown in Fig. 27, less cycles are found for the $\alpha_1 = 0.4$. The reduction of fatigue load experienced by T_s is 12.22%. This shows that the controller has good performance when the load fluctuates under middle wind speed.

Scenario 3: Performance of the system response and fatigue load

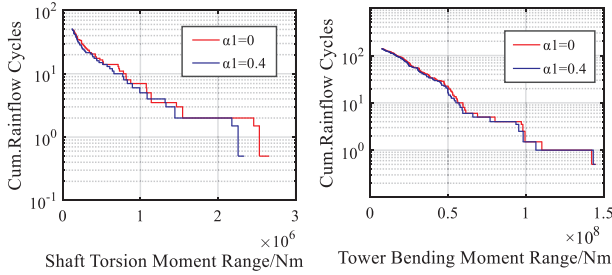


Fig. 27. The cumulative rainflow cycles for T_s and M_t for area 2 under different load disturbances and PID parameters under Mid-speed Section.

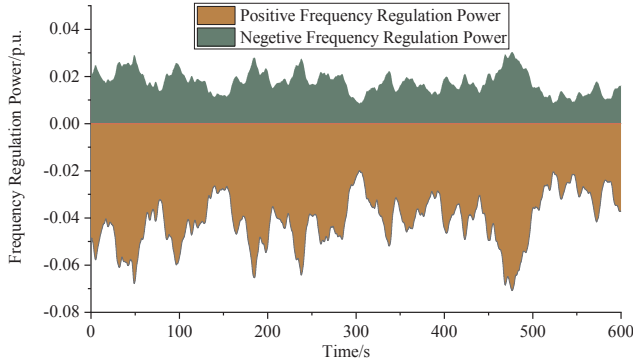


Fig. 28. The positive and negative frequency regulation power of wind power for Low-speed Section.

under Low-speed Section.

In this scenario, the frequency regulation power is shown in Fig. 28. Due to the low wind speed, the available wind power is insufficient. Even if wind power participates in frequency regulation in this case, the effect is not obvious. Simultaneously, the fatigue loads of WT are given in Fig. 29. It can be seen from Fig. 29 that the fatigue loads of WT are lower. They are nearly 10% to 20% of the fatigue loads under High-speed section and Mid-speed section. So, at this time, wind power should be used to generate electricity at maximum power to avoid WT shutdown due to frequency regulation. The impact of wind power fluctuation on the grid frequency and fatigue loads are also small in this scenario.

6. Conclusion

A model identification adaptive PID control method is proposed to improve frequency regulation capability of the power system considering both WT fatigue load and frequency response. The WT model is established for two area LFC model, which the main dynamics of the WT and fatigue load experienced by T_s and M_t can be reflected, and the WT is used to test the proposed method. Through simulation

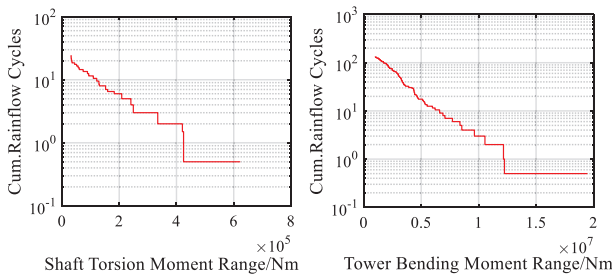


Fig. 29. The cumulative rainflow cycles for T_s and M_t for area 2 under Low-speed Section.

verification, the conclusion are as follows:

- 1) The optimal PID parameters can be optimized by DE algorithm. Step load disturbances with amplitudes of 5, 10 and 15% are applied to test the performance of the controller. The frequency response varies within a small range, which indicates that the model identified adaptive PID control method using the parameters calculated by DE algorithm has a good robustness.
- 2) The frequency response of the system and fatigue load of WT are changed by changing the fatigue load weighting factor α_1 . As α_1 increases, the fatigue load decreases and the frequency response deteriorates. Considering both frequency response and fatigue load, when α_1 is 0.4, the fatigue load is reduced more and the performance of the frequency response is slightly worse. So, $\alpha_1 = 0.4$ is taken as the optimal value.
- 3) The proposed method is tested with three typical conditions. When the wind speed is different, the controller using the optimal PID parameters considering the fatigue load can still make the system have a good frequency response. WT fatigue load is reduced by 0.55% to 32.73% at high-wind speeds compared to controllers that do not consider fatigue loads. WT fatigue load is reduced by 1.62% to 25.70% during Mid-speed Section. And there is no difference in the average output power under different parameters when testing with these two wind speeds. Random load fluctuations are also used to test the performance of the controller. Various results show that the controller can effectively reduce the fatigue load in different wind speed segments, and the benefits of the wind farm will not be affected.

Declaration of Competing Interest

The authors declare that they have no known competing financial interests or personal relationships that could have appeared to influence the work reported in this paper.

Acknowledgments

This work was supported by the National Natural Science Foundation (No. 51677121), the Key Project of National Natural Science Foundation of China (No. 51537007), the Liaoning Provincial Department of Education Serves Local Project (No. LFGD2017009), and the Liaoning Province “Xingliao Yingcai Project” (No. XLYC1802041).

Appendix A. .

The calculation process of the basic differential evolution algorithm.

Step1: The control parameters and specific strategies of DE are determined. The DE control parameters include: population number, mutation operator, crossover operator, maximum evolution algebra, termination condition, etc.

Step2: The initial population is randomly generated, and the evolutionary algebra $t = 1$ s.

Step3: The initial population is evaluated. That is, the fitness value of each individual in the initial population is calculated.

Step4: The program determines whether the termination condition is reached or the evolution algebra reaches the maximum. If the termination condition is reached, the evolution is terminated and the best individual at this time is output as a solution. If the termination condition is not reached, the program continues.

Step 5: The mutation and crossover operations are performed, the boundary conditions are processed, and the temporary population is obtained.

Step6: The temporary population is evaluated, and the fitness value of each individual in the temporary population is calculated.

Step7: The selection operation is performed and the new population is obtained.

Step8: Evolution algebra $t = t + 1$, go to step 4.

Appendix B. Supplementary material

Supplementary data to this article can be found online at <https://doi.org/10.1016/j.ijepes.2019.105696>.

References

- [1] Lenzi A, Steinsland I, Pinson P. Benefits of spatiotemporal modeling for short-term wind power forecasting at both individual and aggregated levels. *Environmetrics* 2018;29(3):e2493.
- [2] Peng S, Jinghao Z, Deqiang G, et al. A rational fractional representation method for wind power integrated power system parametric stability analysis. *IEEE Trans Power Syst* 2018;33(6):7122–31.
- [3] Zhang Z, Zhen L, Kazmierkowski M, et al. Robust predictive control of three-level NPC back-to-back power converter PMSG wind turbine systems with revised predictions. *IEEE Trans Power Electron* 2018;33(11):9588–98.
- [4] Zhao H, Cheng L. Open-switch fault-diagnostic method for back-to-back converters of a doubly fed wind power generation system. *IEEE Trans Power Electron* 2018;33(4):3452–61.
- [5] Kavousi A, Fathi SH, Milimonfared J, et al. Application of boost converter to increase the speed range of dual-stator winding induction generator in wind power systems. *IEEE Trans Power Electron* 2018;33(11):9599–610.
- [6] Datta U, Shi J, Kalam A. Primary frequency control of a microgrid with integrated dynamic sectional droop and fuzzy based pitch angle control. *Int J Elec Power* 2019;111:248–59.
- [7] Prasad S, Purwar S, Kishor N. Non-linear sliding mode control for frequency regulation with variable-speed wind turbine systems. *Int J Elec Power* 2019;107:19–33.
- [8] Ming Z, Zhai J, Li G, et al. Distributed dispatch approach for bulk AC/DC Hybrid systems with high wind power penetration. *IEEE Trans Power Syst* 2018;33(3):3325–36.
- [9] Cao Z, Han Y, Wang J, et al. Two-stage Energy Generation Schedule Market Rolling Optimization of Highly Wind Power Penetrated Microgrids. *Int J Elec Power* 2019;112:12–27.
- [10] Liu Y, Wang Y, Wang X, et al. Active power dispatch for supporting grid frequency regulation in wind farms considering fatigue load. *Energies* 2019;12(8):1508.
- [11] Camblong H, Nourdine S, Vechiu I, et al. Control of wind turbines for fatigue loads reduction and contribution to the grid primary frequency regulation. *Energy* 2012;48(1):284–91.
- [12] Liu Y, Gracia JR, King TJ, et al. Frequency regulation and oscillation damping contributions of variable-speed wind generators in the U.S. eastern interconnection (EI). *IEEE Trans Sustain Energy* 2015;6(3):951–8.
- [13] Wang R, Xie Y, Zhang H, et al. Dynamic power flow algorithm considering frequency regulation of wind power generators. *IET Renew Power Gen* 2017;11(8):1218–25.
- [14] Zhang X, Zha X, Yue S, et al. A Frequency regulation strategy for wind power based on limited over-speed de-loading curve partitioning. *IEEE Access* 2018;6(99):22938–51.
- [15] Morren J, De HS, Kling WL, et al. Wind turbines emulating inertia and supporting primary frequency control. *IEEE Trans Power Syst* 2006;21(1):433–4.
- [16] Zhao J, Lyu X, Fu Y, et al. Coordinated microgrid frequency regulation based on DFIG variable coefficient using virtual inertia and primary frequency control. *IEEE Trans Energy Convers* 2016;31(3):833–45.
- [17] Keung PK, Li P, Banakar H, et al. Kinetic energy of wind-turbine generators for system frequency support. *IEEE Trans Power Syst* 2009;24(1):279–87.
- [18] Arani MFM, Mohamed ARI. Dynamic droop control for wind turbines participating in primary frequency regulation in microgrids. *IEEE Trans Smart Grid* 2018;9(6):5742–51.
- [19] Huang L, Xin H, Zhang L, et al. Synchronization and frequency regulation of DFIG-based wind turbine generators with synchronized control. *IEEE Trans Energy Convers* 2017;32(3):1251–62.
- [20] Liu X, Zhang Y, Lee KY. Coordinated distributed MPC for load frequency control of power system with wind farms. *IEEE Trans Ind Electron* 2017;64(6):5140–50.
- [21] Hasanien HM, El-Fergany AA. Symbiotic organisms search algorithm for automatic generation control of interconnected power systems including wind farms. *IET Gener Transm Dis* 2017;11(7):1692–700.
- [22] Abazari A, Monsef H, Wu B. Load frequency control by de-loaded wind farm using the optimal fuzzy-based PID droop controller. *IET Renew Power Gen* 2019;13(1):180–90.
- [23] Gholamrezaie V, Dozein MG, Monsef H, et al. An optimal frequency control method through a dynamic load frequency control (LFC) model incorporating wind farm. *IEEE Syst J* 2017;12(1):392–401.
- [24] Ana Fernández-Guillamón, Jorge VL, Antonio Viguera-Rodríguez, et al. An adaptive frequency strategy for variable speed wind turbines: application to high wind integration into power. *Systems. Energies* 2018;11(6):1436.
- [25] Fernandez-Guillamon A, Viguera-Rodríguez A, Gomez-Lazaro E, et al. Fast power reserve emulation strategy for VSWT supporting frequency control in multi-area power systems. *Energies* 2018;11(10):2775.
- [26] Jonkman JM, Butterfield S, Musial W, et al. Definition of a 5-MW Reference Wind Turbine for Offshore System Development. Lakewood, CO, USA: National Renewable Energy Lab; 2009.
- [27] Zhao H, Wu Q, Huang S, et al. Fatigue load sensitivity based optimal active power dispatch for wind farms. *IEEE Trans Sustain Energy* 2017;8(3):1247–59.
- [28] Badihi H, Zhang Y, Hong H. Active power control design for supporting grid frequency regulation in wind farms. *Annu Rev Control* 2015;40:70–81.
- [29] Das S, Suganthan PN. Differential evolution: a survey of the state-of-the-art. *IEEE Trans Evol Comput* 2011;15(1):4–31.
- [30] Saad MS, Jamaluddin H, Darus IZM. Implementation of PID controller tuning using differential evolution and genetic algorithms. *Int J Innov Comput I* 2012;8(11):7761–79.
- [31] Grunnet JD, Soltani M, Knudsen T, et al. Aeolus Toolbox for Dynamics Wind Farm Model. Warsaw, Poland: Simulation and Control. The European Wind Energy Conf. & Exihib; Apr. 2010.